

Directional Locking and Hysteresis in Stripe and Bubble Forming Systems on One-Dimensional Periodic Substrates with a Rotating Drive

C. Reichhardt and C. J. O. Reichhardt

*Theoretical Division and Center for Nonlinear Studies,
Los Alamos National Laboratory, Los Alamos, New Mexico 87545, USA*

(Dated: March 12, 2025)

We examine the dynamics of a two-dimensional stripe, bubble, and crystal forming system interacting with a periodic one-dimensional substrate under an applied drive that is rotated with respect to the substrate periodicity direction x . We find that the stripes remain strongly directionally locked to the x direction for an extended range of drives before undergoing motion parallel to the drive. In some cases, the stripes break apart at the unlocking transition, but can dynamically reform into stripes aligned perpendicular to the x direction, producing hysteresis in the directional locking and unlocking transitions. In contrast, moving anisotropic crystal and bubble phases exhibit weaker directional locking and reduced or no hysteresis. The hysteresis occurs in regimes where the particle rearrangements occur and is most pronounced near the stripe phase. We also show that for varied substrate strength, substrate spacing, and particle density, a number of novel dynamical patterns can form that include a combination of stripe, bubble, and crystal morphologies.

I. INTRODUCTION

A wide variety of interacting particle based systems can couple to periodic one-dimensional (1D) substrates, including charged colloids^{1–6}, magnetic skyrmions⁷, dusty plasmas⁸, and vortices in nanostructured type-II superconductors^{9–16}. In these systems, the ordering of the particles depends on both the filling factor and substrate strength, and for certain fillings, the system can form crystal, smectic, or even disordered states. Under driving, the particles remain trapped until a critical depinning force is exceeded. The magnitude of this critical force can oscillate as a function of filling, and for certain fillings, ordered commensurate structures can appear that are more strongly pinned by the substrate^{9,11,15}.

In general, studies of the driven dynamics of particles on 1D substrates are performed with the drive applied perpendicular to the direction of the substrate periodicity. In some studies, however, application of driving over a range of different directions reveals a directional locking effect in which the particles move along the easy flow direction of the substrate regardless of the orientation of the applied drive. When the driving direction is rotated away from the substrate easy flow direction, there is a critical angle above which some of the flow can occur perpendicular to the substrate periodicity direction¹⁶. Additionally, most studies of particles such as colloids or superconducting vortices on 1D substrates have focused only on purely repulsive interparticle interactions that produce a triangular lattice in the absence of a substrate. In a wide variety of particle based systems, more complicated particle-particle interactions are present that lead to the formation of patterns such as stripes, labyrinths, and bubbles, where there can be small scale ordering within individual bubbles or stripes as well as mesoscale ordering of the stripes and bubbles into lattices^{17–26}. These patterned mesophases can arise when the interparticle interaction potential has the short-range attraction and long-range repulsion or SALR form^{21,22,25–32}.

Mesophases can also arise if the interparticle interaction potentials are purely repulsive but have a multi-step shape or contain multiple length scales²⁰. In soft matter, patterned mesophases occur for colloidal systems with various types of competing interactions^{26,28,30,31,33}. In hard condensed matter, mesoscale ordering can occur for vortices in superconducting systems with multiple interaction length scales^{34–39}, magnetic skyrmion-superconducting vortex hybrids⁴⁰, and ordered charges with competing interactions^{41,42}.

When stripe forming systems with SALR interactions are placed on a periodic 1D substrate, the additional periodic modulation of the substrate allows a variety of new types of aligned stripes and mixed bubble-stripe states to form²⁹. In a recent study on the dynamics of a stripe and bubble forming system driven parallel to the periodicity direction of a periodic 1D substrate⁴³, the stripe states were strongly pinned since they could easily align with the substrate, whereas large bubbles were weakly pinned since they could not fit between adjacent substrate maxima. Small bubbles were, however, strongly pinned since they act like point particles that can fit easily between adjacent substrate maxima. As a result, the depinning force was strongly non-monotonic as a function of the strength of the attractive portion of the SALR potential. The depinning threshold increased with increasing attraction in the crystal regime and reached a local maximum in the stripe state before undergoing a large drop at the transition to the large bubble state and then increasing again for small bubbles. When the substrate was sufficiently weak, the stripes exhibited elastic depinning and remained aligned perpendicular to the driving direction. When the substrate was strong, the stripe depinning was plastic and the stripes broke apart but, at higher drives, could dynamically reorder parallel to the drive and perpendicular to the substrate periodicity direction. The bubbles could depin either plastically or elastically, and the transitions between different sliding states for both the stripe and bubble states were associ-

ated with peaks and dips in the velocity-force curves.

In this work, we place SALR systems that form anisotropic crystals, stripes, and bubbles on a 1D periodic substrate and apply an external drive of fixed magnitude along the easy flow or y direction, perpendicular to the substrate periodicity direction. We gradually rotate the drive into the x direction and then into the $-y$ direction. A directional locking or guidance effect appears along the easy ($\pm y$) directions, and there are a series of dynamical phases that emerge as the driving direction is varied. For strong substrates, the most pronounced directional locking occurs for the stripe phase, which exhibits a critical drive angle θ_c at which the particles can jump out of the substrate troughs through the proliferation of kinks or large-scale plastic deformations. After the stripes have broken up and plastically deformed, as the driving angle continues to rotate toward the x direction the particles dynamically reorder into stripes that are oriented along the x direction, parallel to the substrate periodicity direction. As the drive rotates past the x direction and toward the $-y$ direction, the x orientation of the stripes persists past $180^\circ - \theta_c$, leading to strong hysteresis in the directional locking. This hysteresis is the largest in the stripe regime, and is strongly reduced or absent in the bubble and anisotropic crystal phases. We show that a series of dynamical transitions associated with the formation of different patterns appear for the stripe, bubble, and crystal states, and that these transitions produce signatures in the transport, hysteresis, and particle ordering. We map out the dynamic phases for the different patterns as a function of substrate strength, substrate spacing, drive amplitude, and filling.

II. SIMULATION

We model a two-dimensional (2D) system with periodic boundary conditions in the x - and y -directions. The system size is of size L with $L = 36$, and it contains N particles at a density of $\rho = N/L^2$. The interaction potential combines long-range repulsion and short-range attraction. Previously, it was shown that this potential can produce crystals, stripes, void lattices, and bubble lattices depending on the relative strength of the attractive and repulsive terms as well as the particle density^{21,25,27,43}. The dynamics of particle i are obtained by integrating the following overdamped equation of motion:

$$\eta \frac{d\mathbf{R}_i}{dt} = - \sum_{j \neq i}^N \nabla V(R_{ij}) + \mathbf{F}_i^s + \mathbf{F}_D, \quad (1)$$

where $\eta = 1$ is the damping term. The particle-particle interaction potential is

$$V(R_{ij}) = \frac{1}{R_{ij}} - B \exp(-\kappa R_{ij}), \quad (2)$$

where the location of particle $i(j)$ is $\mathbf{R}_{i(j)}$ and $R_{ij} = |\mathbf{R}_i - \mathbf{R}_j|$.

The first term in Eq. (2) is a repulsive Coulomb interaction. It dominates at long distances and also at short distances, so the particles cannot all collapse to a point. The second term is a short-range attraction of strength B that falls off exponentially with a screening length of κ . For fixed ρ and κ , as B increases the system forms crystal, stripe, and clump states, while for fixed B and κ , as ρ increases, the system forms clumps, stripes, void lattices, and a high-density uniform crystal^{25,43}. In this work, we fix $\kappa = 1.0$ while varying B and ρ .

The second term in Eq. (2) is the substrate force, modeled as a sinusoidal potential,

$$\mathbf{F}_s^i = F_p \cos(2\pi x_i/a_p) \quad (3)$$

where x_i is the x position of particle i and the maximum substrate force is F_p . The substrate is composed of N_p minima and has a lattice constant of $a_p = L/N_p$.

After we initialize the particle positions, we apply a driving force given by

$$\mathbf{F}_D = F_D [\cos(\theta)\hat{y} + \sin(\theta)\hat{x}]. \quad (4)$$

Initially, $\theta = 0^\circ$ and the drive is in the $+y$ direction. We then increase θ in increments to a value of 180° , such that when $\theta = 90^\circ$ the drive is aligned with the $+x$ direction, and at the end of our sweep the driving is in the $-y$ direction. Throughout this work we fix $F_D = 1.25$. We also consider a rotating drive in which θ is increased in increments from 0° to 360° repeatedly. As the driving angle is varied, we measure $\langle V \rangle = \sum_i^N \mathbf{v}_i \cdot \hat{x}$ and $\langle V \rangle = \sum_i^N \mathbf{v}_i \cdot \hat{y}$. In general, we find that $\langle V_y \rangle$ exhibits a sinusoidal signature that is in phase with the drive angle, but $\langle V_x \rangle$ shows stronger variations due to the coupling to the substrate.

III. RESULTS

In Fig. 1, we show images from a system with $B = 2.25$, substrate spacing $a_p = 2.067$, and density $\rho = 0.454$. In the absence of a substrate, stripes form that are each two or three particles in width. When the substrate is present but no drive is applied, pinned stripes appear that are a single particle wide, as shown in Fig. 1(a). There are also several void-like features due to the attractive part of the SALR interaction potential. For drive orientations in the range $0 < \theta < 60^\circ$, the system has the same appearance as that shown in Fig. 1(a), but the particles are sliding along the $+y$ direction. In Fig. 2 we plot $\langle V_x \rangle$ versus θ for the same system with no substrate, $F_p = 0.0$, and for a substrate with $F_p = 1.25$. In the presence of the substrate, $\langle V_x \rangle = 0.0$ when $\theta < 60^\circ$, indicating that the motion is locked along the y -direction. The particles have the same structure shown in Fig. 1(a). For $\theta > 60^\circ$, $\langle V_x \rangle$ increases rapidly and reaches a plateau near $\theta = 75^\circ$ followed by a local maximum at $\theta = 90^\circ$. When $\theta > 90^\circ$, $\langle V_x \rangle$ decreases but does not reach zero

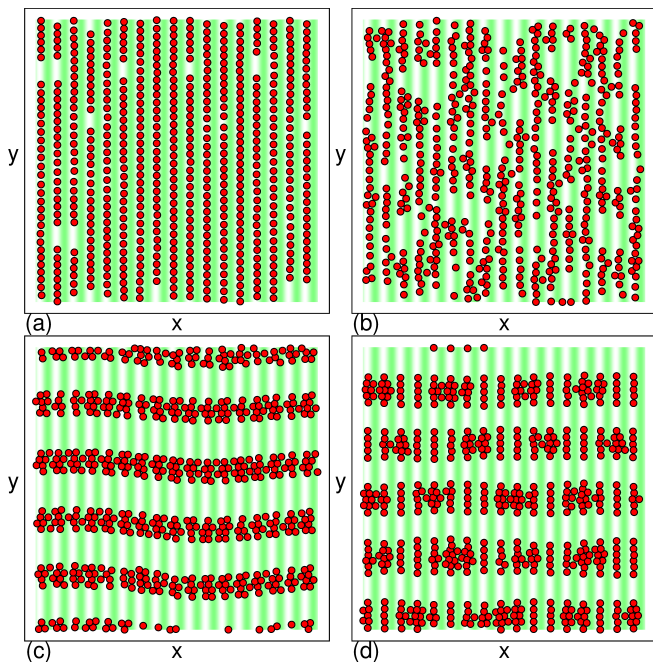


FIG. 1. Particle positions (red circles) and substrate maxima (green) and minima (white) for a system with $B = 2.25$, $F_p = 1.25$, a substrate spacing of $a_p = 2.067$, and $\rho = 0.454$. The drive is initially applied in the $+y$ direction and rotated through the $+x$ direction to the $-y$ direction. (a) A parallel stripe state at $\theta = 0^\circ$ with no drive. (b) A disordered state at $\theta = 66.5^\circ$, just above the drive angle for which the particles begin to move along the x direction. (c) A perpendicular stripe state at $\theta = 90^\circ$ where the driving is purely along the x direction. (d) Persistence of the stripe-like structure at $\theta = 160^\circ$.

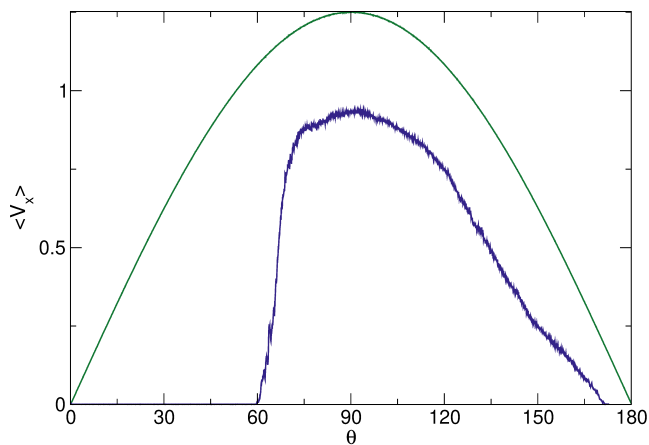


FIG. 2. $\langle V_x \rangle$ vs drive angle θ at $B = 2.25$, $a_p = 2.067$, and $\rho = 0.454$ for the system from Fig. 1 with $F_p = 1.25$ (blue) and $F_p = 0.0$ (green). When $F_p = 0.0$, the velocity response is symmetric about $\theta = 90^\circ$, while for $F_p = 1.25$ the velocity is strongly asymmetric, with the motion remaining locked to the y direction over a much larger range of angles for the $0^\circ < \theta < 90^\circ$ window than for the $90^\circ < \theta < 180^\circ$ window.

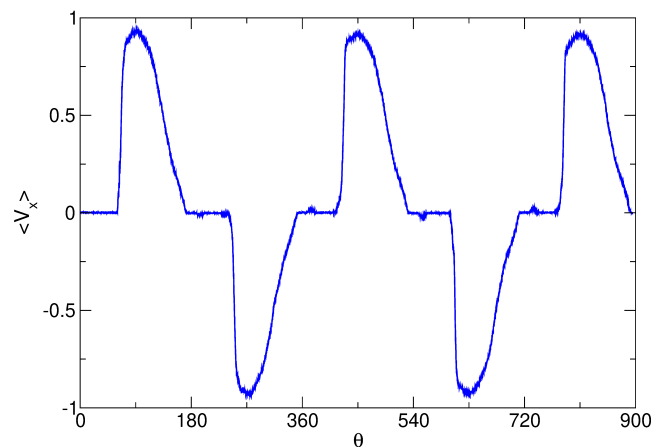


FIG. 3. $\langle V_x \rangle$ vs drive angle θ for the system from Fig. 1 with $B = 2.25$, $F_p = 1.25$, $a_p = 2.067$, and $\rho = 0.454$ for two and a half complete rotations of the drive, showing that the asymmetry in the velocity response persists over multiple drive cycles.

until $\theta = 173^\circ$, showing that there is a strong asymmetry in the velocity response between the $0^\circ < \theta < 90^\circ$ window and the $90^\circ < \theta < 180^\circ$ window. If the response had been symmetric, $\langle V_x \rangle$ would have reached zero near $\theta = 110^\circ$. This asymmetry arises because the particles form different patterns during different stages of the drive orientation. We note that the $\langle V_y \rangle$ response is symmetric, with $\langle V_y \rangle = 1.25$ at $\theta = 0^\circ$ decreasing to $\langle V_y \rangle = -1.25$ at $\theta = 180^\circ$. This is the same response that would be expected for motion in the absence of pinning, since the 1D substrate only affects x direction motion; thus, $\langle V_y \rangle$ has no interesting features for all the cases we consider in this work.

In Fig. 1(b), we illustrate the particle positions at $\theta = 66.5^\circ$, just above the drive angle at which $\langle V_x \rangle$ becomes finite. The system is strongly disordered, and the motion of some particles remains locked along the y direction while other particles move in both the y and x directions, so that a disordered plastic flow state appears. At $\theta = 75^\circ$, the system dynamically orders into an x -oriented stripe state that correlates with the rapid increase in $\langle V_x \rangle$. The x oriented stripes are pictured in Fig. 1(c) at $\theta = 90^\circ$, and as the drive is rotated toward the $-y$ -direction this stripe pattern persists over a range of angles that is wider than the range for which it appeared when the drive was still partially oriented in the $+y$ -direction. As the drive continues to rotate toward the $-y$ direction, the general shape of the stripe remains relatively constant, but an increasing number of particles become pinned in the x direction and have their motion locked along the $-y$ direction, as shown in Fig. 1(d) at $\theta = 160^\circ$. For $\theta = 180^\circ$, the configuration looks the same as the $\theta = 0^\circ$ configuration in Fig. 1(a), but the particles are now moving in the $-y$ direction. If we continue to rotate the drive to values larger than $\theta = 180^\circ$, the same set of patterns and asymmetric responses are repeated,

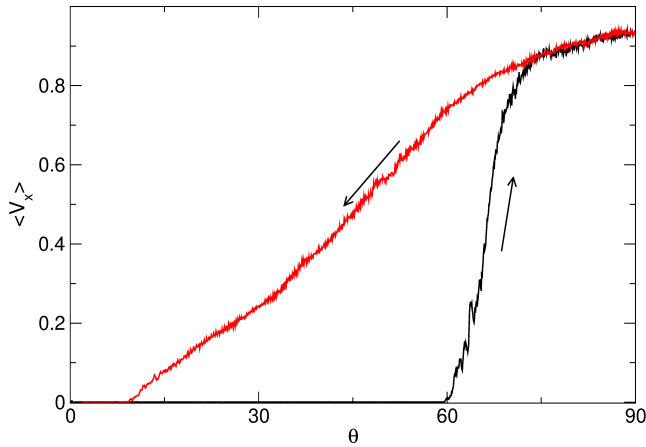


FIG. 4. Hysteretic velocity response for the system from Fig. 1 with $B = 2.25$, $F_p = 1.25$, $a_p = 2.067$, and $\rho = 0.454$. Black: $\langle V_x \rangle$ vs θ for increasing θ from 0° to 90° . Red: Inverted response $\langle V_x \rangle$ vs $90^\circ - \theta$ for θ increasing from 90° to 180° . Inverting the large θ portion of the curve illustrates the hysteresis more clearly.

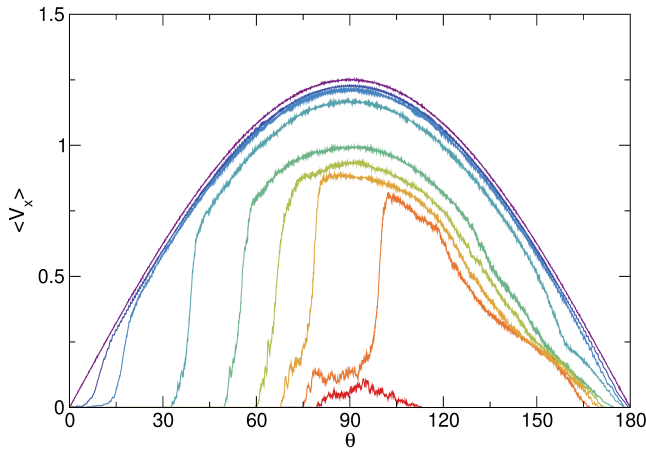


FIG. 5. $\langle V_x \rangle$ vs θ for the system from Fig. 1 with $B = 2.25$, $a_p = 2.067$, and $\rho = 0.454$ at $F_p = 0.0, 0.5, 0.672, 0.875, 1.125, 1.25, 1.325, 1.375, 1.4, \text{ and } 1.5$, from top to bottom. For $F_p > 1.45$, the motion is locked along the $\pm y$ direction for all θ .

as shown in Fig. 3 for the system from Fig. 1 undergoing two and a half complete rotations of the drive. The response remains asymmetric for each drive cycle.

To show more clearly the asymmetry of the hysteresis, in Fig. 4 we plot $\langle V_x \rangle$ versus θ for θ increasing from $\theta = 0^\circ$ to $\theta = 90^\circ$, and overlay an inverted plot of $\langle V_x \rangle$ versus $90^\circ - \theta$ for θ increasing from $\theta = 90^\circ$ to $\theta = 180^\circ$. If the response had been the same on each half of the drive rotation, the curves would follow each other. Instead, we find a strong hysteresis effect, and $\langle V_x \rangle$ is much larger for $\theta > 90^\circ$ than for $\theta < 90^\circ$ due to the persistence of the x -oriented stripe pattern shown in Fig. 1(c,d).

We next consider the evolution of the asymmetry for varied substrate strengths. In Fig. 5, we plot $\langle V_x \rangle$ versus

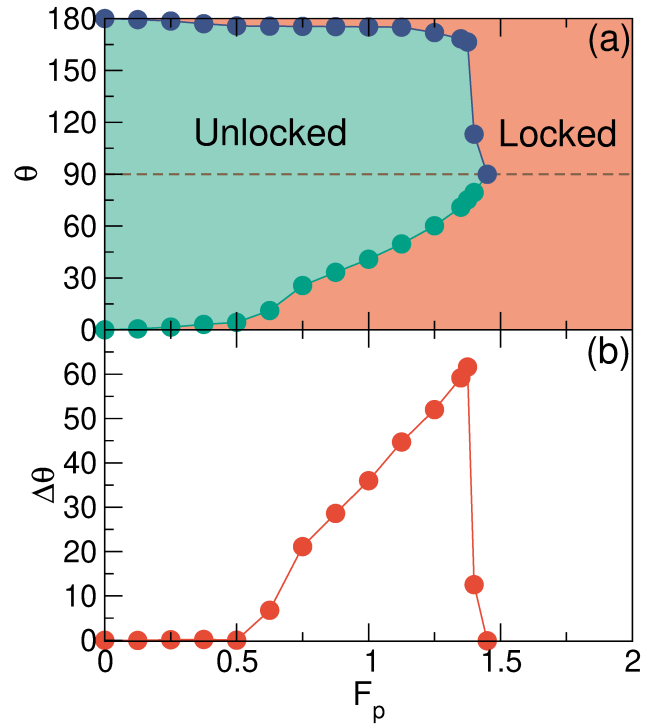


FIG. 6. (a) Boundaries θ_{low} (green) and θ_{hi} (blue) separating the regions where the motion is locked and not locked along the $\pm y$ direction plotted as a function of θ vs F_p for a sample with $B = 2.25$, $a_p = 2.067$, and $\rho = 0.454$. The locked motion is along $+y$ below the dashed line and along $-y$ above the dashed line. (b) $\Delta\theta = \theta_{low} - (180 - \theta_{hi})$ vs F_p for the same system. Larger values of $\Delta\theta$ correspond to a greater amount of hysteresis.

θ for the system from Fig. 1 at $F_p = 0.0, 0.5, 0.672, 0.875, 1.125, 1.25, 1.325, 1.375, 1.4, \text{ and } 1.5$. For $F_p > 1.45$, the motion remains locked along $\pm y$ for all drive angles. When $F_p = 1.4$, there is a small hopping motion along x at drives near $\theta = 90^\circ$. The curves are much more symmetric for $F_p < 0.7$, while at $F_p = 1.375$, the velocity response is strongly asymmetric.

To quantify the evolution of the regions over which the flow is locked along $\pm y$ for increasing F_p , in Fig. 6(a) we plot as a function of θ versus F_p the lower boundary θ_{low} and upper boundary θ_{hi} separating values of θ where $\langle V_x \rangle = 0.0$ and the motion is locked from those where $\langle V_x \rangle$ is finite and the motion is unlocked. The width of the lower locked region increases rapidly for $F_p > 0.5$, and when $F_p > 1.45$, the unlocked region disappears and the motion is always locked to the $\pm y$ direction. We highlight the asymmetry of the locking response in Fig. 5(b), where we plot the difference in width of the $+y$ and $-y$ locking regimes, $\Delta\theta = \theta_{low} - (180 - \theta_{hi})$, versus F_p . If the widths are symmetric, this measure will be zero and there will be no hysteresis. We find that for $F_p < 0.6$, $\Delta\theta = 0$, while for higher F_p , $\Delta\theta$ increases linearly with increasing F_p until it reaches a maximum at $F_p = 1.375$ and then rapidly decreases back to zero at $F_p = 1.45$. For

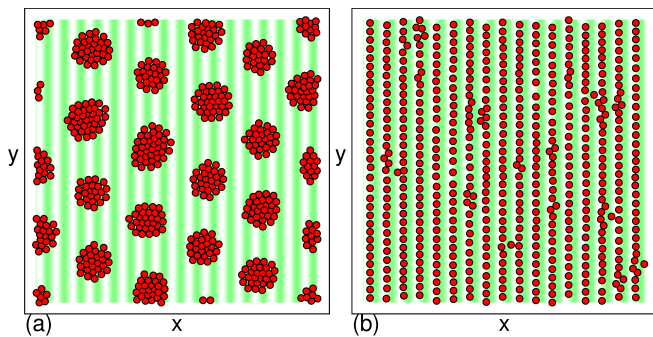


FIG. 7. Particle positions (red circles) and substrate maxima (green) and minima (white) for the system from Fig. 6 with $B = 2.25$, $a_p = 2.067$, and $\rho = 0.454$. (a) The bubble phase at $F_p = 0.5$ and $\theta = 30^\circ$. (b) The locked stripe phase at $F_p = 1.4$ and $\theta = 90^\circ$. A small amount of hopping along the x direction occurs in this state.

$F_p < 0.6$, instead of forming a stripe, the system forms bubbles, as shown in Fig. 7(a) for $\theta = 30^\circ$ and $F_p = 0.5$. At large F_p , the system can no longer form x -direction oriented stripes, and the hysteresis disappears. An example is illustrated in Fig. 7(b) at $F_p = 1.4$ and $\theta = 90^\circ$, where, although some individual particle hopping in x does occur, the particles are mostly pinned along the x direction and there are no x -direction oriented stripes.

By varying the strength B of the attractive term, we next show that the hysteresis is the most produced in the stripe phase. In the absence of a substrate, the SALR particles form an anisotropic crystal for $0 < B < 1.9$, stripes for $2.0 < B < 2.35$, and bubbles for $B > 2.35$. In Fig. 8(a), we plot the boundaries θ_{low} and θ_{high} separating the regions where flow is locked and unlocked in the y direction as a function of θ versus B for a system with $F_p = 1.25$. As B increases, the width of the locked regimes increase, reaching a maximum for $B = 2.25$ at the transition into the stripe state before decreasing nearly to zero. Windows of finite y -direction locking reappear deep in the bubble state for $B > 2.4$. Figure 8(b) shows the corresponding $\Delta\theta$ versus B , which peaks strongly in the stripe phase near $B = 2.25$, not far from the transition to a bubble state. This indicates that by far the most pronounced hysteresis arises in the stripe state. There is still a modest amount of hysteresis in the crystal phase but almost no hysteresis in the bubble phase for $2.5 < B < 3.5$. When $B > 3.5$, the bubbles begin to shrink in size due to the increasing strength of the attractive term, leading to the appearance of some plasticity in the depinning transition and an increase in the hysteresis for the largest values of B considered here.

We next focus on hysteresis in the bubble state. If F_p is large enough, the bubbles break apart into stripes that are oriented in the x direction, and when this happens, hysteresis can occur. In the stripe phase for $B = 2.25$, the motion becomes completely locked to the y direction for $F_p > 1.45$, while in the bubble state at $B = 2.6$,

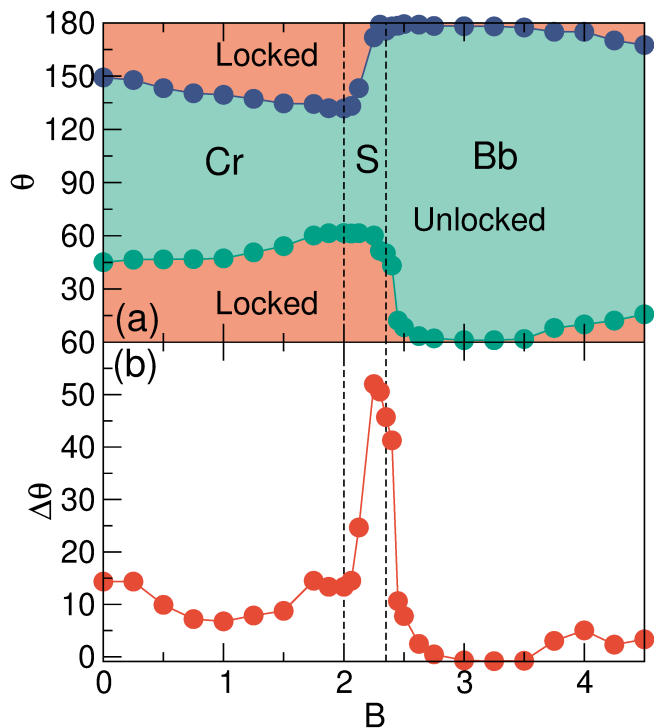


FIG. 8. (a) Boundaries θ_{low} (green) and θ_{hi} (blue) separating the regions where the motion is locked and not locked along the $\pm y$ direction plotted as a function of θ vs B for the system from Fig. 1 with $F_p = 1.25$, $a_p = 2.067$, and $\rho = 0.454$. Dashed lines indicate the values of B at which the system forms crystal (Cr), stripe (S), and bubble (Bb) phases. (b) The corresponding $\Delta\theta$ vs B . The hysteresis is largest in the stripe forming regime.

complete y -direction locking occurs only when $F_p > 3.7$. Figure 9(a) shows the boundaries θ_{low} and θ_{hi} separating the regions in which the motion is locked and not locked to the $\pm y$ direction plotted as a function of θ versus F_p for the system from Fig. 1 in the bubble state at $B = 2.6$. In Fig. 9(b), the corresponding $\Delta\theta$ versus F_p is small for $F_p < 1.5$, where the system remains in a well ordered bubble state for all values of θ . The hysteresis grows with increasing F_p and the system breaks up into a stripe state for $F_p > 2.0$. A maximum in $\Delta\theta$ appears at $F_p = 3.5$, and $\Delta\theta$ drops to zero for $F_p > 3.75$.

In Fig. 10 we plot $\langle V_x \rangle$ versus θ for the $B = 2.6$ system from Fig. 9 at $F_p = 0.0, 0.75, 1.5, 2.0, 2.5, 3.0, 3.125, 3.5, 3.625,$ and 3.75 . The system forms a bubble state at $F_p = 1.25$. The curves are relatively symmetric about $\theta = 90^\circ$ for $F_p < 1.75$, while when $F_p > 1.75$, the curves become increasingly asymmetric, which correlates with the growth in $\Delta\theta$ shown in Fig. 9(b). For $F_p \geq 1.5$, the system forms a y -direction locked stripe of the type shown in Fig. 11(a) at $F_p = 1.5$ and $\theta = 10.0^\circ$. As the drive rotates to higher θ , this stripe state transitions into a bubble state, as shown in Fig. 11(b) for $F_p = 1.5$ and $\theta = 35^\circ$. For $F_p > 1.75$, the system forms a y -direction locked state consisting of x -direction aligned stripes that

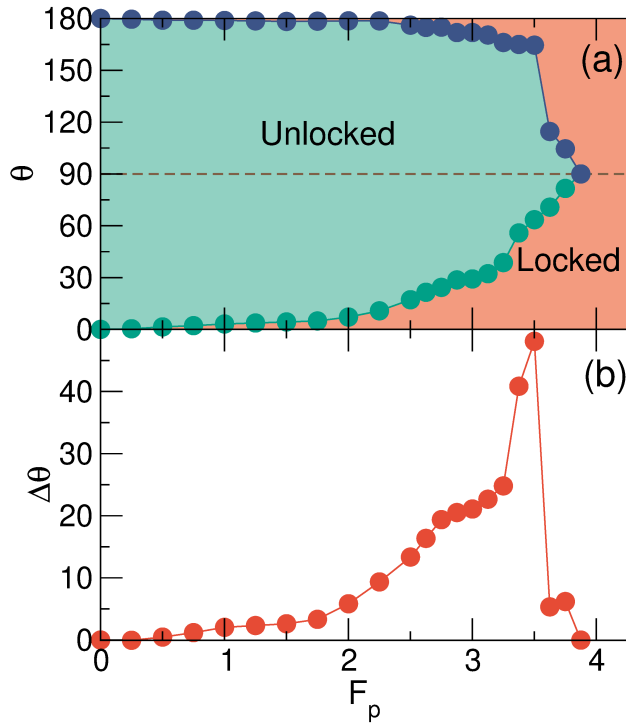


FIG. 9. (a) Boundaries θ_{low} (green) and θ_{hi} (blue) separating the regions where the motion is locked and not locked along the $\pm y$ direction plotted as a function of θ vs F_p for the system from Fig. 1 in the bubble regime with $B = 2.6$, $a_p = 2.067$, and $\rho = 0.454$. (b) The corresponding $\Delta\theta$ vs F_p .

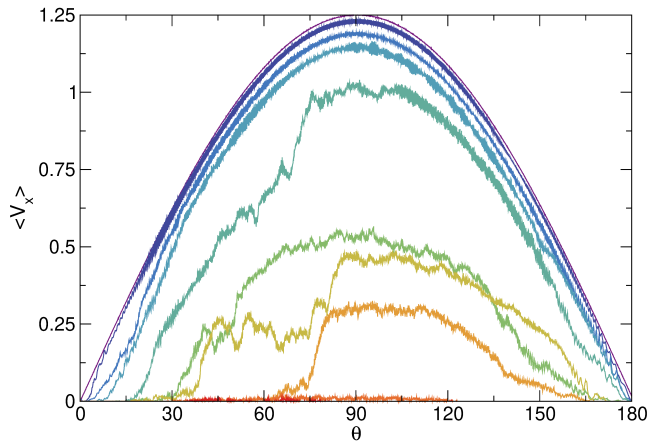


FIG. 10. $\langle V_x \rangle$ vs θ for the bubble forming system from Fig. 9 with $B = 2.6$, $a_p = 2.067$, and $\rho = 0.454$ at $F_p = 0.0, 0.75, 1.5, 2.0, 2.5, 3.0, 3.125, 3.5, 3.625,$ and 3.75 , from top to bottom.

only occupy the substrate troughs, as shown in Fig. 11(c) at $F_p = 3.5$ and $\theta = 0.0^\circ$. As the drive rotates, a portion of the particles begin to move along the x direction by assembling into bubbles that travel along the stripes, as illustrated in Fig. 11(d) at $F_p = 3.5$ and $\theta = 90^\circ$.

To more clearly visualize the dynamics in the $B =$

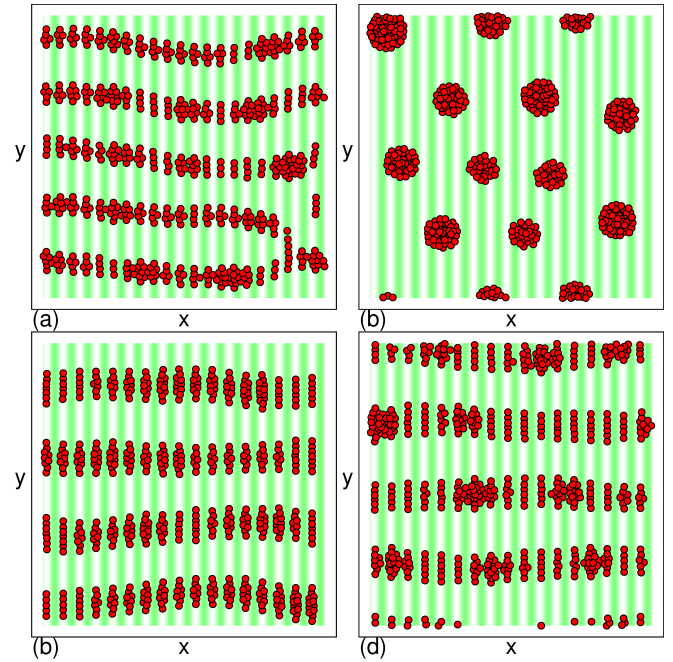


FIG. 11. Particle positions (red circles) and substrate maxima (green) and minima (white) for the system from Fig. 10 with $B = 2.6$, $a_p = 2.067$, and $\rho = 0.454$. (a) $F_p = 1.5$ and $\theta = 10^\circ$. (b) $F_p = 1.5$ and $\theta = 35^\circ$. (c) $F_p = 3.5$ and $\theta = 0.0^\circ$. (d) $F_p = 3.5$ and $\theta = 90^\circ$.

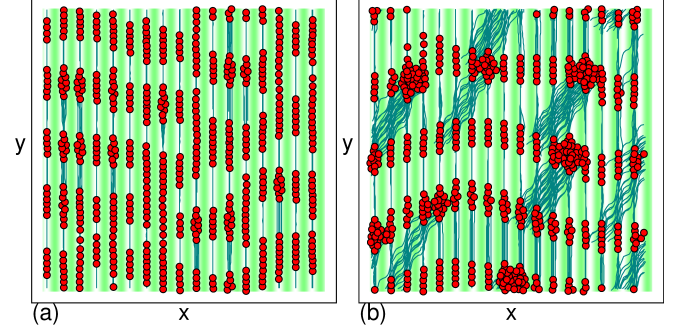


FIG. 12. Particle positions (red circles), substrate maxima (green) and minima (white), and particle trajectories (blue lines) for the system from Fig. 10 with $B = 2.6$, $a_p = 2.067$, $\rho = 0.454$, and $F_p = 3.125$. (a) The locked phase at $\theta = 0.0^\circ$ where the motion is only along the $+y$ direction. (b) The stripe-bubble phase at $\theta = 30^\circ$, where particles in the stripe segments move only along $+y$ while particles in the localized bubbles are moving along both $+x$ and $+y$.

2.6 and $F_p > 1.75$ stripe-bubble coexistence phase that is responsible for the hysteresis peak from Fig. 9(b), in Fig. 12(a) we plot the particle trajectories for a fixed period of time at $F_p = 3.125$ in the y -direction locked regime at $\theta = 0.0^\circ$. Here the particles form a stripe pattern that occupies only the substrate troughs, and the

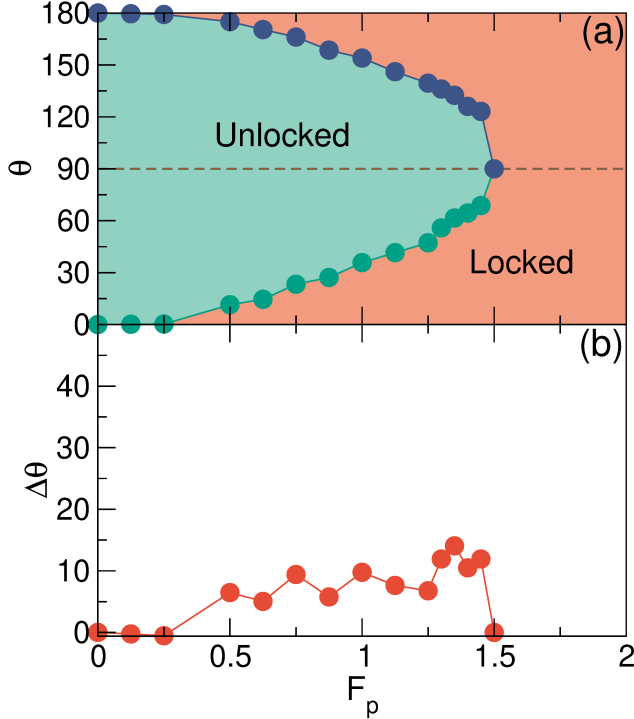


FIG. 13. Boundaries θ_{low} (green) and θ_{hi} (blue) separating the regions where the motion is locked and not locked along the $\pm y$ direction plotted as a function of θ vs F_p for the system from Fig. 8 with $a_p = 2.067$ and $\rho = 0.454$ at $B = 1.0$ in the anisotropic crystal regime. (b) The corresponding $\Delta\theta$ vs F_p , showing strongly reduced hysteresis.

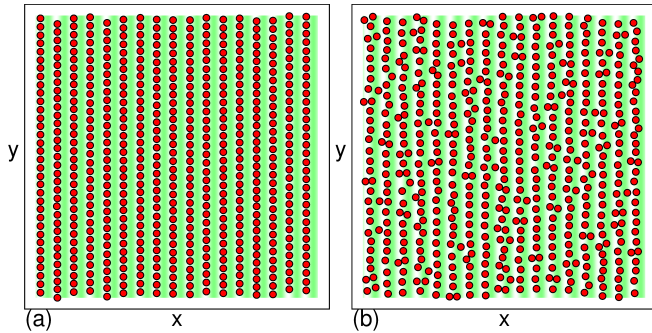


FIG. 14. Particle positions (red circles) and substrate maxima (green) and minima (white) for the system from Fig. 13 with $a_p = 2.067$ and $\rho = 0.454$ in the anisotropic crystal regime at $B = 1.0$ and $F_p = 1.35$. (a) At $\theta = 0.0^\circ$, there is an anisotropic crystal. (b) At $\theta = 90^\circ$, the particles are disordered.

motion is strictly locked to the $+y$ direction. Figure 12(b) shows the same system at $\theta = 30^\circ$, where particles in the striped portions of the system move only along the $+y$ direction, while particles that are inside the localized bubbles move along both the $+x$ and $+y$ directions.

In Fig. 13(a) we plot the boundary separating the

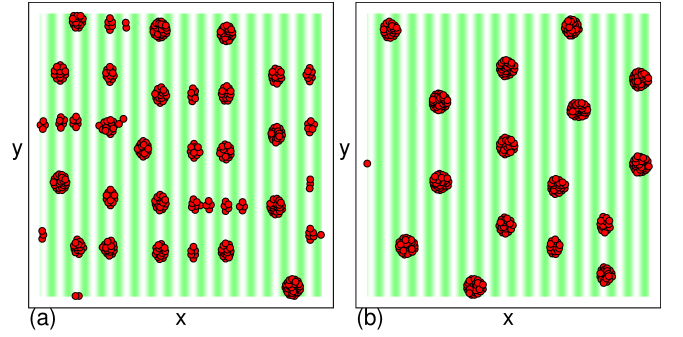


FIG. 15. Particle positions (red circles) and substrate maxima (green) and minima (white) for the system from Fig. 8 with $a_p = 2.067$ and $\rho = 0.454$ at $B = 4.0$ and $F_p = 4.0$. (a) A mixture of stripe segments and bubbles at $\theta = 0.0^\circ$. (b) A bubble state at $\theta = 90^\circ$.

regions of locked and unlocked y -direction motion as a function of θ versus F_p for the system from Fig. 8 at $B = 1.0$ in the anisotropic crystal regime, and in Fig. 13(b) we show the corresponding $\Delta\theta$ versus F_p . The motion becomes locked to the y -direction for all values of θ once $F_p > 1.475$, a threshold that is slightly higher than what we observed for the stripe phase. As indicated by Fig. 13(b), the hysteresis is considerably smaller than what appears in the stripe or bubble phases. In Fig. 14(a) we show the particle positions in the y -direction locked phase at $\theta = 0.0^\circ$ for the system from Fig. 13 at $F_p = 1.35$, where the particles form a uniform anisotropic crystal. At $\theta = 90^\circ$ in the same system, Fig. 14(b) indicates that a disordered state with a uniform density appears. In general, the hysteresis is reduced throughout the anisotropic crystal phases because no dramatic structural transitions occur as the drive is rotated, unlike the large rearrangements that appear for the stripe and bubble states.

We observe reduced hysteresis for other values of B in the crystal phase. In the bubble phase, we find hysteresis only when F_p is large enough to partially break apart some of the bubbles. In Fig. 15(a), we show the particle positions at $B = 4.0$ and $F_p = 4.0$ in the y -direction locked state at $\theta = 0.0^\circ$, where a combination of stripe segments and bubbles are present. In the same system at $\theta = 90^\circ$, shown in Fig. 15(b), an unlocked bubble phase appears. Once the bubbles have assembled, they remain stable out to values of θ that are further from $\theta = 90^\circ$, leading to hysteresis in the locking response.

In Fig. 16, we plot a heat map of $\langle V_x \rangle$ as a function of F_D versus B for a system with $\theta = 90^\circ$. As B increases, the system passes through crystal, stripe, large bubble, and smaller bubble states. The complete locking of the motion along the y direction is the most pronounced in the crystal and stripe phases for $F_p > 1.5$. In the large bubble regime for $3.0 < B < 3.9$, no y direction locking occurs up to at least $F_p = 5.0$. At larger B , there is a partial reentrance in the y direction locking when the

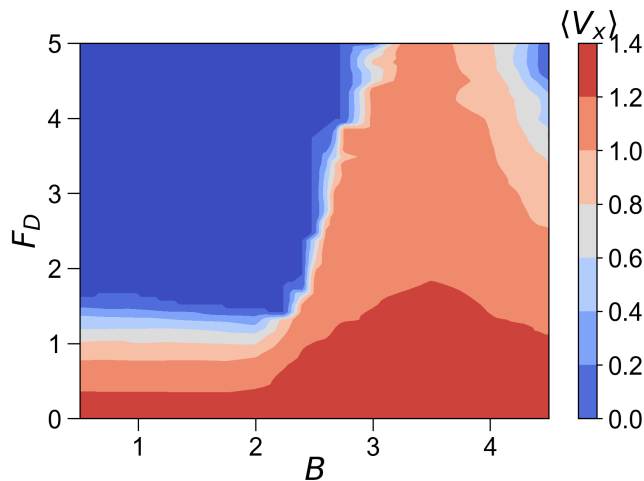


FIG. 16. Heat map of $\langle V_x \rangle$ as a function of F_D vs B for a system with $a_p = 2.067$, $\rho = 0.454$, and $\theta = 90^\circ$. The system passes through crystal, stripe, large bubble, and small bubble states with increasing B .

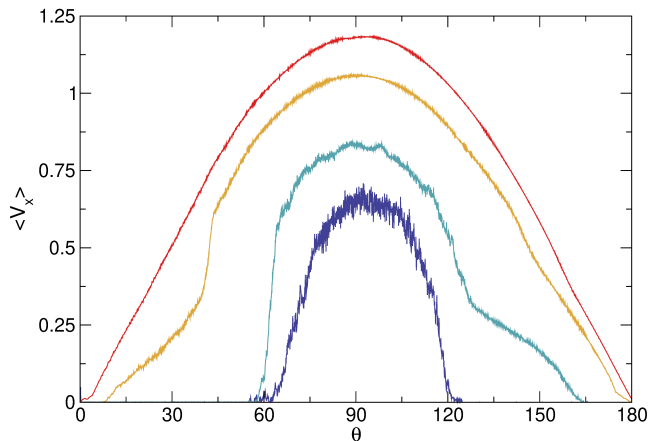


FIG. 17. $\langle V_x \rangle$ vs θ for a system with $B = 2.25$, $F_p = 1.25$, and $a_p = 2.067$ at $\rho = 0.164, 0.33, 0.682$, and 1.32 , from bottom to top.

bubbles decrease in size and become better pinned by the substrate troughs, since the smaller bubbles act more like point particles than the larger bubbles do.

IV. VARIED PARTICLE DENSITY

We next consider the effect of varying the particle density ρ for the system from Fig. 1 with $B = 2.25$ and $F_p = 1.25$. In Fig. 17 we plot $\langle V_x \rangle$ versus θ at $\rho = 0.164, 0.33, 0.682$, and 1.32 . When $\rho = 0.164$, there are large windows of θ over which $\langle V_x \rangle = 0.0$, and the curve is nearly completely symmetric about $\theta = 90^\circ$. In contrast, the response is strongly asymmetric for $\rho = 0.33$, which has an extended finite $\langle V_x \rangle$ velocity tail for $\theta > 90^\circ$. The $\rho = 0.682$ curve is more symmetric, and has a clear jump

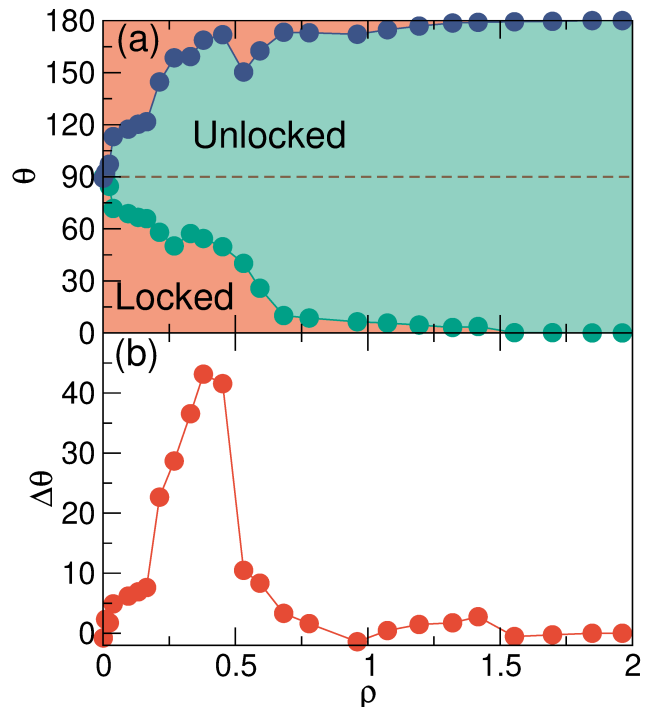


FIG. 18. Boundaries θ_{low} (green) and θ_{hi} (blue) separating the regions where the motion is locked and not locked along the $\pm y$ direction plotted as a function of θ vs ρ for the system from Fig. 17 with $B = 2.25$, $a_p = 2.067$, and $F_p = 1.25$. (b) The corresponding $\Delta\theta$ vs ρ .

up in $\langle V_x \rangle$ near $\theta = 35^\circ$. For $\rho = 1.32$, the particle-particle interactions begin to overwhelm the substrate interactions, and the curve becomes nearly symmetric with no y -direction locking windows.

In Fig. 18(a) we plot the boundaries separating the locked and unlocked y -direction motion regimes as a function of θ versus F_p in the system from Fig. 17. Figure 18(b) shows the corresponding $\Delta\theta$ versus F_p . At low particle densities, thin stripes or small bubbles are present, giving a window of reduced hysteresis. For $0.19 < \rho < 0.52$, we find strong hysteresis when the system forms an aligned stripe phase as the driving direction approaches 90° . For high densities, a stripe-bubble coexistence phase is present. In general, when $F_p = 1.25$, the pinning is strongly reduced at the higher densities, so the amount of hysteresis is reduced even though structural transitions may still occur as the drive is rotated.

In Fig. 19(a), we show the coexisting stripe-bubble state from the system in Fig. 17 at $\rho = 0.68$ and $\theta = 20^\circ$. The motion of the particles in the striped portion of the system is locked along the $+y$ direction, while the particles in the bubbles move along both the $+x$ and $+y$ directions. At $\theta = 90^\circ$, the system forms stripes that are well-aligned in the x direction and that are composed of bubbles that are elongated in the y direction, as shown in Fig. 19(b). The jump up in $\langle V_x \rangle$ that occurs near $\theta = 30^\circ$ in Fig. 17 for the $\rho = 0.68$ sample coincides with a tran-

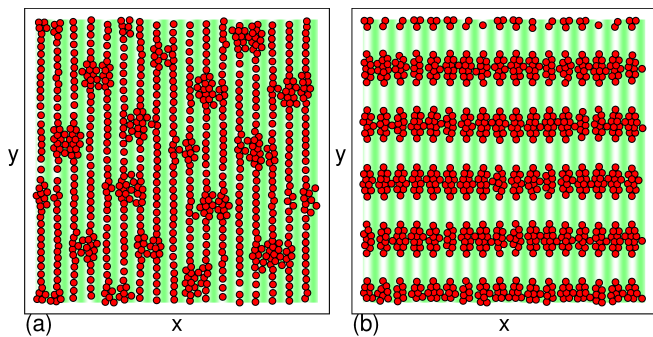


FIG. 19. Particle positions (red circles) and substrate maxima (green) and minima (white) for the system from Fig. 17 with $a_p = 2.067$, $B = 2.25$, $F_p = 1.25$, and $\rho = 0.68$. (a) The stripe-bubble phase at $\theta = 20^\circ$. (b) The stripe phase at $\theta = 90^\circ$.

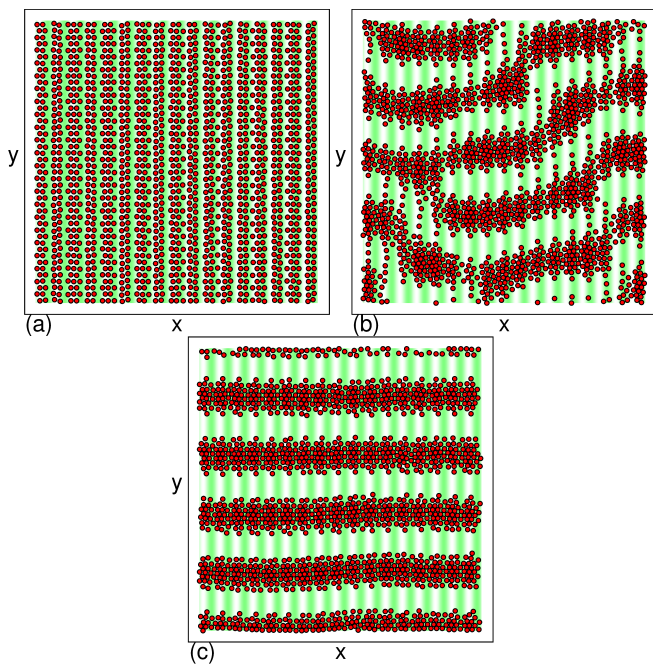


FIG. 20. Particle positions (red circles) and substrate maxima (green) and minima (white) for the system from Fig. 17 with $a_p = 2.067$, $B = 2.25$, $F_p = 1.25$, and $\rho = 1.32$. The circles representing the particles are drawn with a reduced radius compared to the images obtained at lower ρ . (a) y -aligned stripes at $\theta = 0.0^\circ$. (b) A disordered stripe state at $\theta = 15^\circ$. (c) x -aligned stripes at $\theta = 90^\circ$.

sition from the stripe-bubble state to the stripe state. In this case, simply measuring hysteresis according to $\Delta\theta$, which is based on the locking of the velocity to the $\pm y$ direction, gives a small hysteresis value; however, inspection of the actual finite value of $\langle V_x \rangle$ reveals that strong velocity hysteresis is present.

In Fig. 20(a), we show the particle configurations at

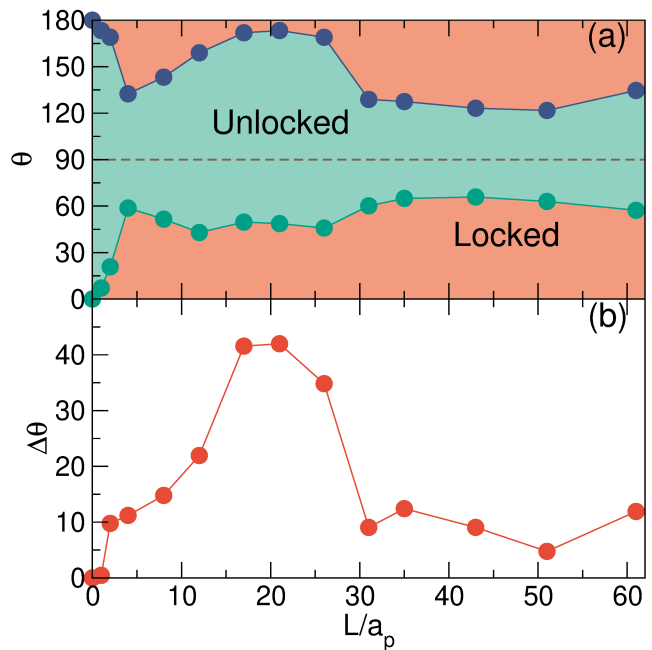


FIG. 21. (a) Boundaries θ_{low} (green) and θ_{hi} (blue) separating the regions where the motion is locked and not locked along the $\pm y$ direction plotted as a function of θ vs L/a_p for a system with $B = 2.25$, $F_p = 1.25$, and $\rho = 0.454$. (b) The corresponding $\Delta\theta$ vs L/a_p .

$\theta = 0.0^\circ$ for the $\rho = 1.32$ system from Fig. 17 where y -aligned stripes appear. At $\theta = 15^\circ$ in Fig. 20(b), the aligned stripes break apart and the system begins to assemble into disordered stripes that are partially aligned in the x direction. For $\theta = 90^\circ$ in Fig. 20(c), the stripes have become well aligned along the x direction. Even though a structural transition occurs in this system, there is only weak hysteresis since the effectiveness of the pinning is relatively weak. For $\rho > 1.57$ (not shown), the system forms a uniform crystal that undergoes almost no structural change as the drive is rotated, and the hysteresis vanishes.

V. VARIED SUBSTRATE SPACING

In Fig. 21(a), we plot the boundaries θ_{low} and θ_{hi} separating the regions of y -locked motion from unlocked motion for a system with $F_p = 1.25$ and $B = 2.25$ as a function of θ versus L/a_p , the number of substrate minima. We note that up until this point, we have presented results from systems where $a_p = 2.067$ and $L/a_p = 17$. Figure 21(b) shows the corresponding $\Delta\theta$ versus L/a_p , where we find strong hysteresis for $10 < L/a_p < 30$. In the hysteretic regime, the particles form stripes or labyrinths that are aligned in the y direction, while for larger values of L/a_p corresponding to smaller values of a_p , the system forms stripes that are aligned in the x direction. In the latter regime, fewer structural rearrange-

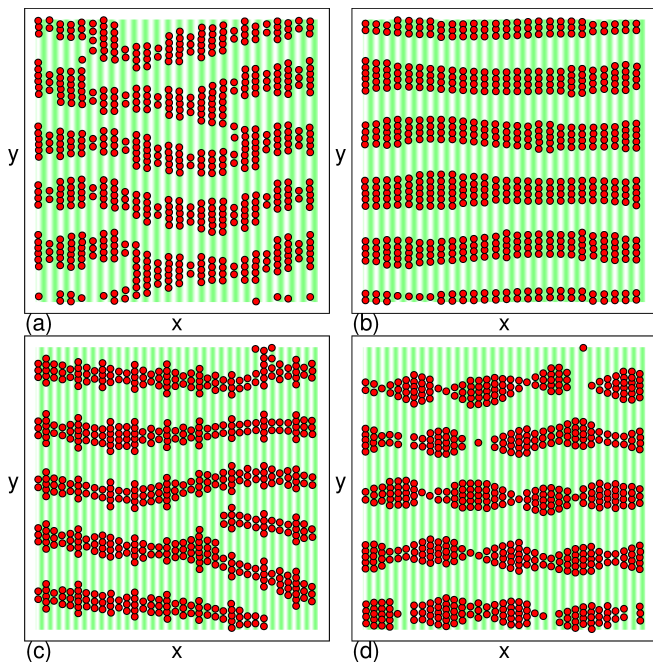


FIG. 22. Particle positions (red circles) and substrate maxima (green) and minima (white) for the system from Fig. 21 with $B = 2.25$, $F_p = 1.25$, and $\rho = 0.454$. (a) A labyrinthine pattern at $L/a_p = 26$ and $\theta = 0.0^\circ$. (b) A stripe state at $L/a_p = 26$ $\theta = 90^\circ$. (c) A stripe state at $L/a_p = 35$ and $\theta = 0^\circ$. (d) A stripe state at $L/a_p = 35$ and $\theta = 180^\circ$.

ments occur as the drive is rotated, so the hysteresis is reduced. For $L/a_p < 10$ at $\theta = 0.0^\circ$, although the stripes are aligned with the y direction, each stripe is multiple particles wide, which reduces the effectiveness of the substrate pinning and thus diminishes the amount of hysteresis that appears.

In Fig. 22(a), we show a labyrinth-like phase that forms for $L/a_p = 26$ when $\theta = 0.0^\circ$, and in Fig. 22(b) we show a stripe state at $\theta = 90^\circ$ for the same system. For this substrate spacing, pronounced hysteresis arises since the structure changes significantly as the drive is rotated. The ordered stripe phase illustrated in Fig. 22(b) has $\theta_{\text{low}} > 180 - \theta_{\text{hi}}$, and persists over a wider range of θ as the drive is rotated into the $-y$ direction for $\theta > 90^\circ$. In Fig. 22(c), we show the stripe phase at $\theta = 0.0^\circ$ for $L/a_p = 35$, where the hysteresis is reduced. In the same system at $\theta = 180^\circ$, Fig. 22(d) indicates that a stripe state is still present. Although some rearrangements of the stripes occur as the drive is rotated, the general structure and orientation of the stripes remains unchanged,

reducing the amount of hysteresis that occurs.

VI. SUMMARY

We have examined the symmetry locking and dynamic phases for crystal, stripe, and bubble forming systems interacting with a one-dimensional periodic substrate that has its periodicity along the x direction under a drive that is rotated from the $+y$ direction to the $-y$ direction. Here, the particle-particle interactions are composed of a combination of long-range repulsion and short-range attraction. We measure the range of drive angles over which the motion remains locked along the y direction, and find that in regimes where stripes are present that are initially aligned with the y direction, the directional locking of the motion under the rotating drive is the strongest. The y -aligned stripes can dynamically reorder into wider x -aligned stripes, resulting in strongly asymmetric velocity versus angle curves and a hysteretic response to the drive. The asymmetry of the response persists even if multiple rotations of the drive are performed, and occurs because the x alignment of the stripes persists longer during the $-y$ phase of the drive rotation than during the $+y$ phase of the drive rotation. The hysteresis is generally reduced in the bubble and crystal phases. When the substrate is very strong, the bubble phase can also show pronounced hysteresis when the flow consists of a bubble-stripe mixture where the stripe portion of the particles have their motion locked along the y direction but the bubble portion of the particles move in both the x and y directions. In the crystal phases, the hysteresis is always strongly reduced. For higher particle densities, the system can undergo structural transitions, but the locking effects are strongly reduced when the density becomes high enough to cause the stripes to grow very wide.

ACKNOWLEDGMENTS

We gratefully acknowledge the support of the U.S. Department of Energy through the LANL/LDRD program for this work. This work was supported by the US Department of Energy through the Los Alamos National Laboratory. Los Alamos National Laboratory is operated by Triad National Security, LLC, for the National Nuclear Security Administration of the U. S. Department of Energy (Contract No. 892333218NCA000001).

¹ A. Chowdhury, B. J. Ackerson, and N. A. Clark, “Laser-induced freezing,” *Phys. Rev. Lett.* **55**, 833–836 (1985).

² J. Chakrabarti, H. R. Krishnamurthy, A. K. Sood, and S. Sengupta, “Reentrant melting in laser field modulated

colloidal suspensions,” *Phys. Rev. Lett.* **75**, 2232–2235 (1995).

³ Q.-H. Wei, C. Bechinger, D. Rudhardt, and P. Leiderer, “Experimental study of laser-induced melting in

- two-dimensional colloids,” *Phys. Rev. Lett.* **81**, 2606–2609 (1998).
- ⁴ L. Radzihovsky, E. Frey, and D. R. Nelson, “Novel phases and reentrant melting of two-dimensional colloidal crystals,” *Phys. Rev. E* **63**, 031503 (2001).
 - ⁵ J. Baumgartl, M. Brunner, and C. Bechinger, “Locked-floating-solid to locked-smectic transition in colloidal systems,” *Phys. Rev. Lett.* **93**, 168301 (2004).
 - ⁶ L. Zaidouny, T. Bohlein, R. Roth, and C. Bechinger, “Light-induced phase transitions of colloidal monolayers with crystalline order,” *Soft Matter* **9**, 9230–9236 (2013).
 - ⁷ C. Reichhardt and C. J. Olson Reichhardt, “Magnus-induced dynamics of driven skyrmions on a quasi-one-dimensional periodic substrate,” *Phys. Rev. B* **94**, 094413 (2016).
 - ⁸ K. Wang, W. Li, D. Huang, C. Reichhardt, C. J. O. Reichhardt, M. S. Murillo, and Y. Feng, “Structures and diffusion of two-dimensional dusty plasmas on one-dimensional periodic substrates,” *Phys. Rev. E* **98**, 063204 (2018).
 - ⁹ P. Martinoli, “Static and dynamic interaction of superconducting vortices with a periodic pinning potential,” *Phys. Rev. B* **17**, 1175–1194 (1978).
 - ¹⁰ G. I. Watson and G. S. Canright, “Frustration-induced disorder of flux-line structures in layered superconductors,” *Phys. Rev. B* **48**, 15950–15956 (1993).
 - ¹¹ V. A. Shklovskij and O. V. Dobrovolskiy, “Influence of pointlike disorder on the guiding of vortices and the Hall effect in a washboard planar pinning potential,” *Phys. Rev. B* **74**, 104511 (2006).
 - ¹² O. V. Dobrovolskiy, E. Begun, M. Huth, and V. A. Shklovskij, “Electrical transport and pinning properties of Nb thin films patterned with focused ion beam-milled washboard nanostructures,” *New J. Phys.* **14**, 113027 (2012).
 - ¹³ I. Guillamón, R. Córdoba, J. Sesé, J. M. De Teresa, M. R. Ibarra, S. Vieira, and H. Suderow, “Enhancement of long-range correlations in a 2D vortex lattice by an incommensurate 1D disorder potential,” *Nature Phys.* **10**, 851–856 (2014).
 - ¹⁴ O. V. Dobrovolskiy, M. Hanefeld, M. Zörb, M. Huth, and V. A. Shklovskij, “Interplay of flux guiding and Hall effect in Nb films with nanogrooves,” *Supercond. Sci. Technol.* **29**, 065009 (2016).
 - ¹⁵ Q. Le Thien, D. McDermott, C. J. Olson Reichhardt, and C. Reichhardt, “Orientational ordering, buckling, and dynamic transitions for vortices interacting with a periodic quasi-one-dimensional substrate,” *Phys. Rev. B* **93**, 014504 (2016).
 - ¹⁶ O. V. Dobrovolskiy, V. M. Bevez, E. Begun, R. Sachser, R. V. Vovk, and M. Huth, “Fast dynamics of guided magnetic flux quanta,” *Phys. Rev. Applied* **11**, 054064 (2019).
 - ¹⁷ M. Seul and D. Andelman, “Domain shapes and patterns - the phenomenology of modulated phases,” *Science* **267**, 476–483 (1995).
 - ¹⁸ C. Harrison, D. H. Adamson, Z. Cheng, J. M. Sebastian, S. Sethuraman, D. A. Huse, R. A. Register, and P. M. Chaikin, “Mechanisms of ordering in striped patterns,” *Science* **290**, 1558–1560 (2000).
 - ¹⁹ A. D. Stoycheva and S. J. Singer, “Computer simulations of a two-dimensional system with competing interactions,” *Phys. Rev. E* **65**, 036706 (2002).
 - ²⁰ G. Malescio and G. Pellicane, “Stripe phases from isotropic repulsive interactions,” *Nature Mater.* **2**, 97–100 (2003).
 - ²¹ C. Reichhardt, C. J. Olson, I. Martin, and A. R. Bishop, “Depinning and dynamics of systems with competing interactions in quenched disorder,” *Europhys. Lett.* **61**, 221–227 (2003).
 - ²² K. Nelissen, B. Partoens, and F. M. Peeters, “Bubble, stripe, and ring phases in a two-dimensional cluster with competing interactions,” *Phys. Rev. E* **71**, 066204 (2005).
 - ²³ Y. H. Liu, L. Y. Chew, and M. Y. Yu, “Self-assembly of complex structures in a two-dimensional system with competing interaction forces,” *Phys. Rev. E* **78**, 066405 (2008).
 - ²⁴ E. Edlund and M. N. Jacobi, “Universality of striped morphologies,” *Phys. Rev. Lett.* **105**, 137203 (2010).
 - ²⁵ C. J. Olson Reichhardt, C. Reichhardt, and A. R. Bishop, “Structural transitions, melting, and intermediate phases for stripe- and clump-forming systems,” *Phys. Rev. E* **82**, 041502 (2010).
 - ²⁶ A. Hooshanginejad, J.-W. Barotta, V. Spradlin, G. Pucci, R. Hunt, and D. M. Harris, “Interactions and pattern formation in a macroscopic magnetocapillary salt system of mermaid cereal,” *Nature Commun.* **15**, 5466 (2024).
 - ²⁷ C. J. O. Reichhardt, C. Reichhardt, I. Martin, and A. R. Bishop, “Dynamics and melting of stripes, crystals, and bubbles with quenched disorder,” *Physica D* **193**, 303–309 (2004).
 - ²⁸ J.-X. Chen, J.-W. Mao, S. Thakur, J.-R. Xu, and F. Liu, “Dynamical phase of driven colloidal systems with short-range attraction and long-range repulsion,” *J. Chem. Phys.* **135**, 094504 (2011).
 - ²⁹ D. McDermott, C. J. Olson Reichhardt, and C. Reichhardt, “Stripe systems with competing interactions on quasi-one dimensional periodic substrates,” *Soft Matter* **10**, 6332–6338 (2014).
 - ³⁰ C. P. Royall, “Hunting mermaids in real space: known knowns, known unknowns and unknown unknowns,” *Soft Matter* **14**, 4020–4028 (2018).
 - ³¹ Y. Liu and Y. Xi, “Colloidal systems with a short-range attraction and long-range repulsion: phase diagrams, structures, and dynamics,” *Curr. Opin. Colloid Interf. Sci.* **19**, 123–136 (2019).
 - ³² X. B. Xu, T. Tang, Z. H. Wang, X. N. Xu, G. Y. Fang, and M. Gu, “Nonequilibrium pattern formation in circularly confined two-dimensional systems with competing interactions,” *Phys. Rev. E* **103**, 012604 (2021).
 - ³³ L. Q. Costa Campos, S. W. S. Apolinario, and H. Löwen, “Structural ordering of trapped colloids with competing interactions,” *Phys. Rev. E* **88**, 042313 (2013).
 - ³⁴ E. Babaev and M. Speight, “Semi-Meissner state and neither type-I nor type-II superconductivity in multicomponent superconductors,” *Phys. Rev. B* **72**, 180502 (2005).
 - ³⁵ X. B. Xu, H. Fangohr, Z. H. Wang, M. Gu, S. L. Liu, D. Q. Shi, and S. X. Dou, “Vortex dynamics for low- κ type-II superconductors,” *Phys. Rev. B* **84**, 014515 (2011).
 - ³⁶ J. Gutierrez, B. Raes, A. V. Silhanek, L. J. Li, N. D. Zhigadlo, J. Karpinski, J. Tempere, and V. V. Moshchalkov, “Scanning Hall probe microscopy of unconventional vortex patterns in the two-gap MgB₂ superconductor,” *Phys. Rev. B* **85**, 094511 (2012).
 - ³⁷ L. Komendová, M. V. Milošević, and F. M. Peeters, “Soft vortex matter in a type-I/type-II superconducting bilayer,” *Phys. Rev. B* **88**, 094515 (2013).
 - ³⁸ P. J. Curran, W. M. Desoky, M. V. Milosevic, A. Chaves, J. B. Laloe, J. S. Moodera, and S. J. Bending, “Spontaneous symmetry breaking in vortex systems with two

- repulsive lengthscales,” *Sci. Rep.* **5**, 15569 (2015).
- ³⁹ Q. Meng, C. N. Varney, H. Fangohr, and E. Babaev, “Phase diagrams of vortex matter with multi-scale inter-vortex interactions in layered superconductors,” *J. Phys.: Condens. Matter* **29**, 035602 (2017).
- ⁴⁰ J. F. Neto and C. C. de Souza Silva, “Mesoscale phase separation of skyrmion-vortex matter in chiral-magnet-superconductor heterostructures,” *Phys. Rev. Lett.* **128**, 057001 (2022).
- ⁴¹ J. M. Tranquada, B. J. Sterlieb, J. D. Axe, Y. Nakamura, and S. Uchida, “Evidence for stripe correlations of spins and holes in copper-oxide superconductors,” *Nature (London)* **375**, 561–563 (1995).
- ⁴² C. J. Olson Reichhardt, C. Reichhardt, and A. R. Bishop, “Fibrillar templates and soft phases in systems with short-range dipolar and long-range interactions,” *Phys. Rev. Lett.* **92**, 016801 (2004).
- ⁴³ C. Reichhardt and C. J. O. Reichhardt, “Peak effect and dynamics of stripe- and pattern-forming systems on a periodic one-dimensional substrate,” *Phys. Rev. E* **109**, 054606 (2024).